Harmonic Current Suppression Strategy for Grid-Connected PWM Converters with LCL Filters

Zhao, Rende; Li, Qian; Xu, Hailiang; Wang, Yansong; Guerrero, Josep M.

Published in:
IEEE Access

DOI (link to publication from Publisher):
10.1109/ACCESS.2019.2893226

Publication date:
2019

Document Version
Publisher's PDF, also known as Version of record

IEEE Access
Multidisciplinary | Rapid Review | Open Access Journal

Received December 19, 2018, accepted January 3, 2019, date of publication January 18, 2019, date of current version February 12, 2019.

Digital Object Identifier 10.1109/ACCESS.2019.2893226

Harmonic Current Suppression Strategy for Grid-Connected PWM Converters With LCL Filters

RENDE ZHAO[1], (Member, IEEE), QIAN LI[1], HAILIANG XU[1], (Member, IEEE), YANSONG WANG[1], AND JOSEP M. GUERRERO[2], (Fellow, IEEE)

[1]College of Information and Control Engineering, China University of Petroleum (East China), Qingdao 266580, China
[2]Department of Energy Technology, Aalborg University, 9220 Aalborg, Denmark

Corresponding author: Hailiang Xu (xuhl@zju.edu.cn)

This work was supported in part by the National Natural Science Foundation of China under Grant 51507190 and Grant 51677193.

ABSTRACT As for a grid-connected PWM converter with LCL filter, harmonic current can flow freely into the grid-side inductor and filter capacitor, when the connected power grid is harmonically distorted. The fact lies in that the conventional control scheme has a little ability to suppress the grid current harmonics. Though the harmonics can be suppressed by the capacitor current compensation method, it may lead to system stability issues. This paper proposes an improved harmonic suppression scheme with the partial capacitor current feedforward, which can effectively suppress the specified grid current harmonics on the premise of ensuring the system stability. Since the partial capacitor current is obtained as the differential output of a multi-second-order generalized integrator, no extra current sensors are needed. The effectiveness and feasibility of the proposed strategy are verified by detailed experimental results.

INDEX TERMS Grid-connected converter, LCL filter, harmonic current, resonant control.

I. INTRODUCTION

LCL filters are broadly applied in the grid-connected PWM converters to filter out the high-frequency harmonics of the grid currents [1]–[3]. Compared with the L filter, the LCL filter has better high-frequency harmonic attenuation capability [4], [5]. The control algorithms of the grid-connected PWM converter with LCL filter can be simply classified into two categories, i.e., converter current feedback (CCF) control and grid current feedback (GCF) control [6]. As shown in Fig. 1, when the selected switch turns to i_1, the CCF control is adopted, with its feedback of the closed-loop control system being the converter-side current; when the selected switch turns to i_2, however, the GCF control is triggered, with the grid side current being its feedback. The CCF control is widely used in industrial products due to its convenience of the overcurrent protection [8]. Furthermore, under the weak grid conditions, the CCF control system is easy to keep stable because of its inherent impedance characteristics [9]. However, the GCF control system, usually needs to introduce an auxiliary damping control to ensure the system stability [10]–[14].

As for the harmonic current suppression capability, it has been proved that with CCF control system, harmonic current can flow into the capacitor freely [15], [16], if the grid voltage is harmonically distorted. The experimental waveforms of the grid voltage, the grid current and the capacitor current the PWM converter with the CCF control are shown in Fig. 2. Obviously, the currents are seriously distorted because the grid voltage has some harmonic components, i.e., the grid-background harmonics. As illustrated in Fig. 1, no grid-background harmonic information is included in the CCF control loop, which is why it cannot suppress the grid-side harmonic currents.

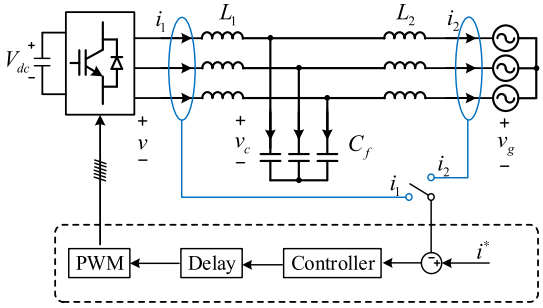

FIGURE 1. Block diagram of CCF control and GCF control.

A lot of work has been done to improve the harmonic suppression capability of the CCF control [7], [8], [17]. In [7], a grid voltage proportional feedforward strategy was proposed. It shows a better harmonic suppression capability

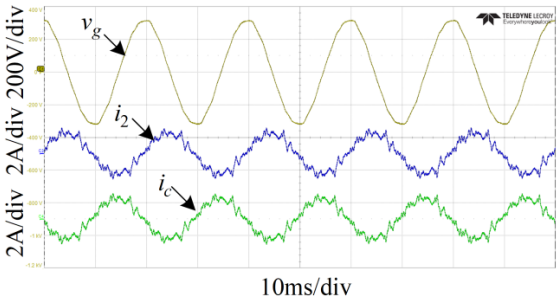

FIGURE 2. Experimental waveforms of the grid voltage, the grid current and the capacitor current.

when the system delay is not considered. However, the delay is inevitable in the digital control system, which may lead to the instability of the system. Then, Butterworth low-pass filter and the repetitive controller were proposed for the delay compensation to improve the system stability, which introduce the complexity and parameter sensitivity issues. In [17], a low-pass filter was adopted in the grid voltage feedforward loop to ensure the system stability. Taking the low-pass filter's amplitude and the phase errors into account, the grid current may still be distorted. In [8], the grid voltage feedforward transfer function was obtained, which fully reduced the influence of grid background harmonics on the grid current. However, the function contained a second order differentiator that was sensitive to high frequency noises. In addition, the capacitor current was needed in the feedforward scheme [8], which increased the cost of the extra current sensors. A simple way to suppress the harmonics may be to feed forward all the capacitor current to the current reference in the CCF control. Nevertheless, the CCF control turns to be equivalent to the GCF control in such design, which may cause system instability [18].

This paper thus proposes a novel improved control scheme based on the CCF control system to suppress the grid-side harmonic current caused by the grid-background harmonics. A partial capacitor current compensation method is proposed, with the specified harmonic currents feedforward. A multi-second-order generalized integrator (MOSGI) is utilized to extract the specified harmonic currents from the voltage of the capacitor. Hence, no extra current sensors are needed. The proposed control strategy possesses the stability characteristic of the CCF control and harmonic suppression capability of the GCF control, simultaneously.

This paper is organized as follows. Section II describes the conventional CCF control system by modeling the grid harmonic impedance. In Section III, the capacitor current extraction method based on MSOGI is presented in detail. To suppress the grid-background harmonics, an enhanced CCF control scheme is developed in section IV. Besides, the system stability with the proposed scheme is discussed. The experimental tests are then performed in Section V to validate the effectiveness and feasibility of the proposed strategy. Finally, some useful conclusions are summarized in Section VI.

II. MODEL AND PROBLEM ANALYSIS OF CONVENTIONAL CCF CONTROL SYSTEM

A. MODEL OF CONVENTIONAL CCF CONTROL SYSTEM

Fig. 3(a) shows the topology of a LCL-filtered grid-connected converter with the conventional CCF control. The LCL filter consists of a converter-side inductor L_1, grid-side inductor L_2 and filter capacitor C_f. Fig. 3(b) presents the equivalent block diagram of the conventional CCF control. The current controller herein is a proportional–resonant (*PR*) controller [19] plus a group of harmonic controllers (*HCs*). And the *HCs* consists of multiple resonant controllers, with their resonant frequencies at the harmonic frequencies. The transfer function of the combined current controller can be represented as follows.

$$G_c(s) = K_p + \frac{K_{r1}s}{s^2 + \omega'^2} + \sum_{h}^{J} \frac{K_{rh}s}{s^2 + h^2\omega'^2} \tag{1}$$

where K_p, ω', K_{r1}, h, K_{rh} and J respectively denote the proportional gain, the fundamental frequency, the resonant gain of fundamental component, the harmonic order, the resonant gain of each harmonic component, and the maximum harmonic order to be suppressed.

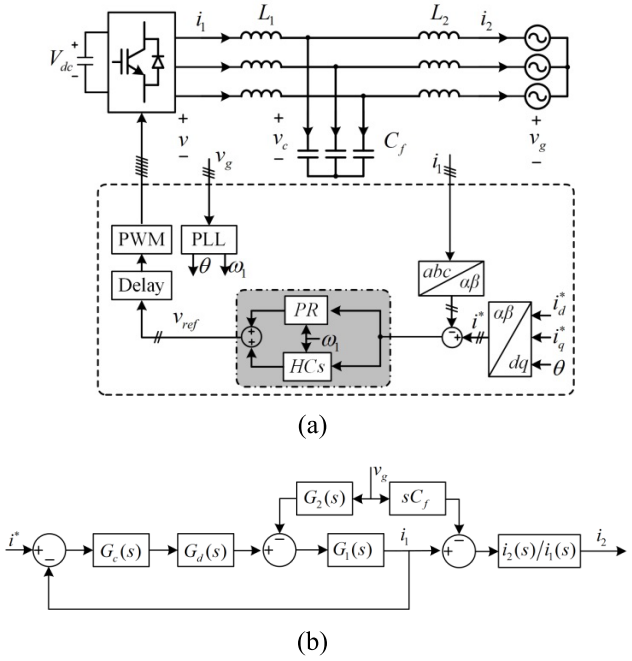

FIGURE 3. Three-phase LCL-filtered grid-connected converter. (a) topology of converter with conventional CCF control, (b) equivalent block diagram of conventional CCF control.

In the s-domain, the converter control delay can be described as

$$G_d(s) = e^{-T_d s} \tag{2}$$

where T_d is the system total time delay, which can be approximated as 1.5 T_s [6] by considering the process of sampling, computation, compare registers update, and zero-order-hold of the Pulse-Width Modulation (PWM) [20].

According to Fig. 3, the open-loop transfer function of the system can be obtained as

$$T_1(s) = G_c(s)G_d(s)G_1(s) \tag{3}$$

The converter current and grid current can be extracted from the reference current and the grid voltage, which can be separately expressed as

$$i_1 = \frac{G_c(s)G_d(s)G_1(s)}{1 + G_1(s)G_c(s)G_d(s)} i^* - \frac{G_1(s)G_2(s)}{1 + G_1(s)G_c(s)G_d(s)} v_g \tag{4}$$

$$i_2 = \frac{G_c(s)G_d(s)G_1(s)G_2(s)}{1 + G_1(s)G_c(s)G_d(s)} i^* - \left(\frac{G_1(s)G_2^2(s)}{1 + G_1(s)G_c(s)G_d(s)} + sC_f G_2(s) \right) v_g \tag{5}$$

where $G_1(s) = \frac{s^2L_2C_f+1}{s^3L_1L_2C_f+s(L_1+L_2)}$, $G_2(s) = \frac{1}{s^2L_2C_f+1}$.

B. HARMONIC IMPEDANCE ANALYSIS

To elaborate grid-current harmonic attenuation ability, the grid harmonic impedance can be established to evaluate the relationship between the grid voltage and the resulting grid current [18]. It has been proved that the sensitivity of a converter control system to the harmonics of the grid voltage can be investigated by calculating its harmonic impedance [8]. In response to a harmonic voltage disturbance, higher harmonic impedance will lead to a smaller harmonic current. Thus, it is an effective way to evaluate the harmonic disturbance rejection capability of the system [8]. The grid harmonic impedance of conventional CCF control system can be extracted from (4) as

$$z_g = \frac{v_g}{i_2} = \frac{s^3L_1L_2 + s(L_1 + L_2) + \left[1 + s^2L_2C_f\right] G_c(s)G_d(s)}{1 + s^2L_2C_f + sC_f G_c(s)G_d(s)} \tag{6}$$

At harmonic frequencies, G_c (s) has infinite gain by *HCs*. As a result, (6) can be simplified as

$$z_{g\_harmonic} \approx sL_2 + \frac{1}{sC_f} \tag{7}$$

According to (7), the harmonic impedance exhibits both inductive characteristic and capacitive characteristic, which is determined by the grid-side inductor L_2 and filter capacitor C_f. The characteristic can also be descripted by the equivalent circuit model [21], as shown in Fig. 4, where the controller is regarded as a parallel branch formed by a set of LC circuits. At the harmonic frequencies, the impedance of the LC circuit becomes infinite, which blocks the harmonic current flowing into loop1. Consequently, the harmonic current mainly flows in loop2 though L_2 and C_f.

The Bode diagrams of the grid harmonic impedance are given in Fig. 5 with the *HCs* (5th, 7th, 11th and 13th orders)

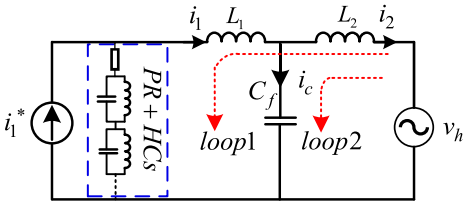

FIGURE 4. Equivalent impedance model of the LCL-filtered grid-connected converter with conventional CCF control.

being enabled and disabled, respectively. Here the fundamental resonant controller is disabled in order to distinguish the difference caused by the *HCs*. The controller parameters, i.e., K_p and K_{rh}, are properly designed according to [22].

As shown in Fig. 5, the harmonic impedance magnitude with *HCs* enabled is slightly larger than that of the disabled condition at harmonic frequencies. However, the harmonic impedance magnitudes in the two conditions are both below 50dB, which would show a limited harmonic suppression capability. This is because the *HCs* can only suppress the harmonic current in loop1 in Fig. 4 but has no effect on the harmonic current in loop2. It can thus be concluded that the CCF control system with *HCs* can attenuate harmonic current caused by distorted grid voltage partially but not completely due to the lack of the grid harmonic current information.

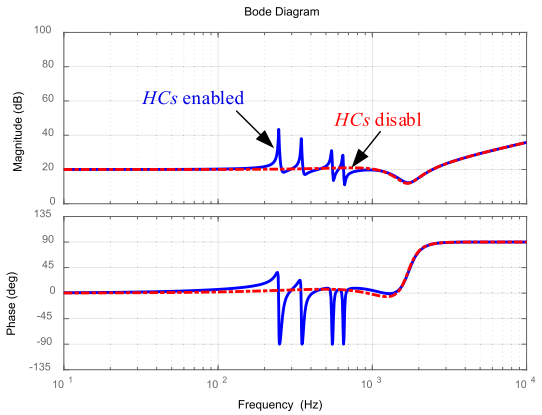

FIGURE 5. Bode diagrams of the harmonic impedance in conventional CCF control system with HCs enabled and disabled.

Therefore, to eliminate the grid harmonic currents, the lacked harmonic information should be compensated into the CCF control system. Since the grid harmonic currents flow through the filter capacitor directly, the capacitor current contains all the harmonic information which can be selected as the compensation references. Hence, it becomes a crucial issue to extract the capacitor current accurately and expediently.

III. CAPACITOR CURRENT EXTRACTION BASED ON MSOGI

In term of capacitor current sampling, the current sensor has the advantages of convenient and high precision, but

the cost is considerable. As we know, the capacitor current is the differentiation of its voltage. Hence a differentiator can be applied to the capacitor voltage to extract its current component, which could reduce the cost. A digital differentiator based on second-order generalized integrator (SOGI) is explored in the paper. Note that the proposed control system is not so sensitive to the magnitude error introduced by the digital differentiator, since such error can be eliminated by the integration characteristic of the resonant controllers.

In practice, the grid voltage may contain harmonics at various frequencies, with several of them dominating the voltage distortion. Furthermore, the digital system has severe distortion of high-order harmonic sampling because the sampling rate is always limited. Hence, it is not necessary to extract all the capacitor current. The SOGI has an infinite gain at its resonant frequency [23] and such characteristic can be applied to extract the capacitor current at the harmonic frequencies.

A. PRINCIPLE OF THE CAPACITOR CURRENT EXTRACTION BASED ON SOGI

The SOGI structure is shown in Fig. 6, where ω' is the turning frequency, and k is the gain, v_c' is the observation signal with the same magnitude and phase as the input signal v_c. d_v_c' is the differential of v_c.

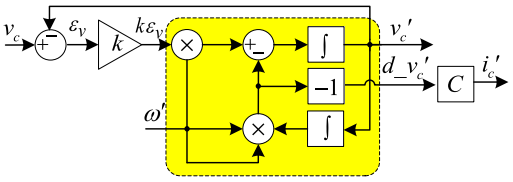

FIGURE 6. Structure of SOGI.

Assume the capacitor voltage to be

$$v_c = A\sin(\omega' t) \tag{8}$$

Then there are

$$v_c' = A\sin(\omega' t) \tag{9}$$

and

$$d\_v_c' = \omega' A\cos(\omega' t) \tag{10}$$

The capacitor current can be expressed as

$$i_c' = C\frac{dv_c'}{dt} = C\omega' A\cos(\omega' t) \tag{11}$$

From (10) and (11), the capacitor current can be given as

$$i_c' = Cd\_v_c' \tag{12}$$

Consequently, the capacitor current can be extracted by the digital differentiator based on SOGI, and the transfer function between the capacitor current and the capacitor voltage can be represented as

$$I_{C1}(s) = \frac{i_c'(s)}{v_c(s)} = -C\frac{k\omega'^3}{s^2+\omega'^2} \tag{13}$$

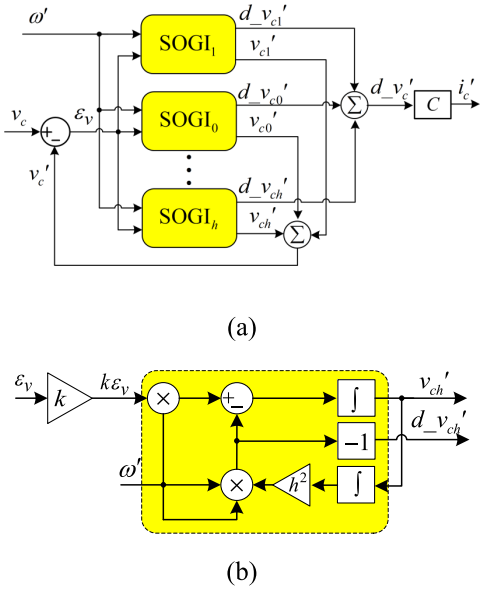

FIGURE 7. Scheme of the capacitor current extraction based on MSOGI. (a) scheme of MSOGI, (b) normalized structure of SOGI.

B. EXTRACTION OF THE CAPACITOR HARMONIC CURRENTS BASED ON MSOGI

The former section illustrates the principle of extracting fundamental component of capacitor current based on SOGI. In fact, it can be effectively explored to extract the harmonic capacitor current as well by a parallel SOGI structure, i.e., MSOGI. The diagram of the MSOGI-based capacitor harmonic currents extraction is shown in Fig. 7(a). Fig. 7(b) shows the normalized structure the SOGI, and h representing the harmonic order.

According Fig. 7(b), the transfer function of the observation signal to the system error can be obtained as

$$B_h(s) = \frac{v_{ch}'(s)}{\varepsilon_v(s)} = \frac{k\omega' s}{s^2+h^2\omega'^2} \tag{14}$$

And the transfer function of the system error to the input signal can be achieved as

$$\begin{aligned} N(s) &= \frac{\varepsilon_v}{v_c}(s) = \frac{1}{1+B_0(s)+B_1(s)+\cdots} \\ &= \frac{1}{1+\sum\limits_{h=0,1,\cdots} B_h(s)} \end{aligned} \tag{15}$$

Synthetic (14) and (15), the transfer function between the output in-phase signal and the input signal can be obtained as

$$M_h(s) = \frac{v_{ch}'}{v_c}(s) = \frac{B_h(s)}{1+\sum\limits_{h=0,1,\cdots} B_h(s)} \tag{16}$$

And the transfer function between the output differential signal and the input signal can be then represented as

$$L_h(s) = \frac{d\_v_{ch}'}{v_c}(s) = -\frac{h^2\omega'^2}{s}\frac{B_h(s)}{1+\sum\limits_{h=0,1,\cdots} B_h(s)} \tag{17}$$

As a result, the transfer function between the sum of the extracted capacitor current and the capacitor voltage can be given by

$$I_C(s) = C \sum_{h=0,1,\cdots} L_h(s) \tag{18}$$

To verify the current extraction accuracy, the Bode diagram of equation (18) is presented in Fig. 8, where $\omega' = 100\pi$, $C = 10\mu F$, $k = \sqrt{2}$ and $h = 0, 1, 5, 7$. At the harmonic frequencies, the theoretical amplitude gains are$20\lg(\omega' C) = -50.1dB$, $20\lg(5\omega' C) = -36.1dB$, $20\lg(7\omega' C) = -33.2dB$, respectively. Explicitly, the obtained amplitude gains from the Bode diagram are very well consistent with the theoretical calculated ones. So the accuracy of the current extraction method is initially demonstrated.

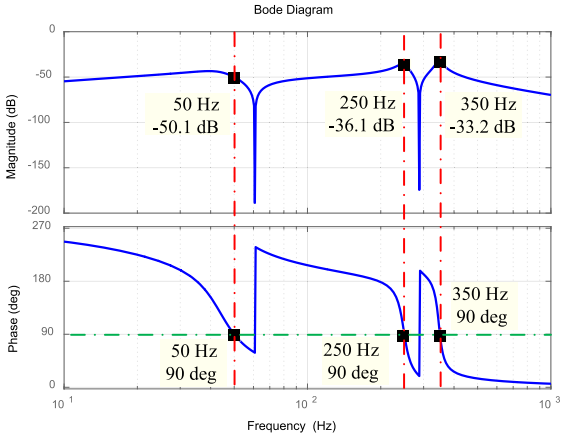

FIGURE 8. Bode diagram of transfer function of capacitor current and capacitor voltage.

IV. CCF CONTROL SCHEME WITH PARTIAL CAPACITOR CURRENT FEEDFORWARD

In order to suppress the grid current harmonics effectively and ensure the stability of the system simultaneously, a CCF based control scheme with partial capacitor current feedforward is put forward. The partial capacitor current contains the fundamental component and selected order harmonics to be suppressed.

A. MODEL OF CCF CONTROL SYSTEM WITH PARTIAL CAPACITOR CURRENT FEEDFORWARD

The whole control block diagram of the proposed scheme is shown in Fig. 9, where the capacitor current is extracted by the MSOGI. According to the diagram, the open loop transfer function of the system can be derived as

$$T_1'(s) = \frac{G_c(s)G_d(s)G_1(s)}{1 - G_c(s)G_d(s)G_{vc}I(s)} \tag{19}$$

where $G_{vc} = \frac{v_c(s)}{i_1(s)} = \frac{L_2}{s^2L_1L_2C_f + L_1 + L_2}$.

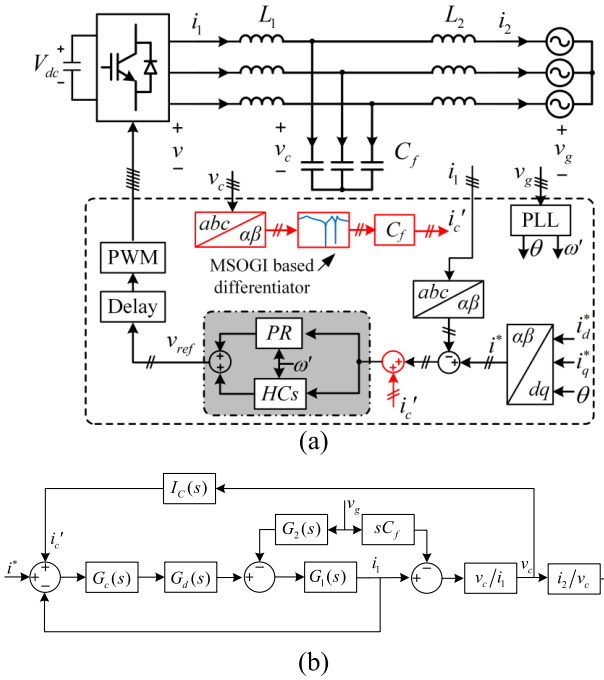

FIGURE 9. Three-phase LCL-filtered grid-connected converter. (a) topology of converter with proposed CCF control scheme, (b) equivalent block diagram of proposed CCF control.

The grid current can be extracted from the reference current and grid voltage, which can be expressed as

$$i_2 = \frac{G_c(s)G_d(s)G_1(s)G_2(s)}{1 - [G_3(s)G_5(s) - G_1(s)]G_c(s)G_d(s)} \times i^* - \left(\frac{G_1(s)G_2^2(s) - G_5(s)G_c(s)G_d(s)G_4(s)G_2(s)}{1 - [G_3(s)G_5(s) - G_1(s)]G_c(s)G_d(s)} + sC_fG_2(s) \right) v_g \tag{20}$$

where $G_1 = \frac{s^2L_2C_f+1}{s^3L_1L_2C_f+s(L_1+L_2)}$, $G_2 = \frac{1}{s^2L_2C_f+1}$, $G_3 = \frac{s^2L_2C_f}{s^3L_1L_2C_f+s(L_1+L_2)}$, $G_4 = \frac{sC_f}{s^3L_1L_2C_f+s(L_1+L_2)}$, $G_5(s) = \frac{I_C(s)}{sC_f}$.

B. HARMONIC IMPEDANCE ANALYSIS

To elaborate the grid-current harmonic attenuation ability of the proposed control scheme, the grid harmonic impedance is firstly derived from (20), which can be obtained as

$$\frac{v_g}{i_2} = \frac{s^3L_1L_2 + s(L_1+L_2) + \left[1 + s^2L_2C_f\left(1 - \frac{I_C(s)}{sC_f}\right)\right] G_c(s)G_d(s)}{s^2L_2C_f + 1 + sC_fG_c(s)G_d(s)\left(1 - \frac{I_C(s)}{sC_f}\right)} \tag{21}$$

At harmonic frequencies, the partial capacitor current is accurately extracted by MSOGI, i.e., $I_C(s)/sC_f \approx 1$; then the grid harmonic impedance is mainly determined by *HCs*.

As a result, the transfer function can be simplified as

$$\frac{v_g}{i_2} \approx \frac{K_{rh}}{s^2 + h^2\omega'^2} \tag{22}$$

From (22), it can be seen that infinite gains can be obtained at the resonant frequencies, which means infinite resistances for the grid harmonic currents.

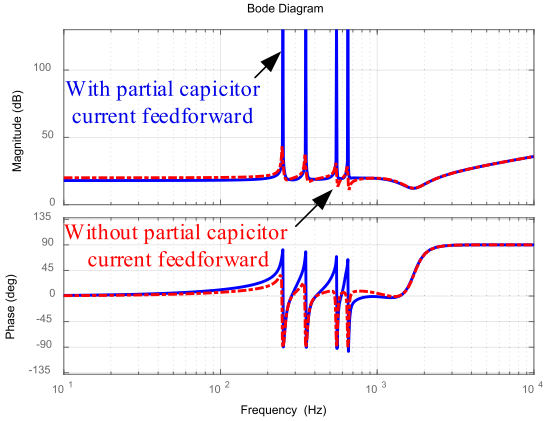

FIGURE 10. Bode diagram of the grid harmonic impedance for the CCF control system when partial capacitor current feedforward is enabled and disabled.

Fig. 10 illustrates the bode diagram of the grid harmonic impedance for the CCF control system when partial capacitor current feedforward is enabled and disabled. $G_c(s)$ is configured to be resonant at the 5th, 7th, 11th and 13th order harmonics, while the fundamental resonant controller is disabled in order to clearly distinguish the difference caused by the harmonic controller. It can be seen that the*HCs* shows a satisfactory harmonic attenuation ability with the grid harmonic information indirectly provided by the partial capacitor current. However, as for the conventional CCF control, the impedance is always below 50dB, which means that the harmonic attenuation ability is limited. It thus can be concluded that the proposed scheme is superior to the conventional CCF control scheme on the harmonic suppression capability.

Though the proposed control behaves well in the grid harmonic current suppression, it is known that the CCF based control scheme with all capacitor current feedforward can lead to system instability. Considering that the proposed control scheme equals to GCF control scheme in some extent. It is necessary to discuss the system stability effected by partial capacitor current feedforward.

C. STABILITY ANALYSIS OF CCF CONTROL SYSTEM WITH PARTIAL CAPACITOR CURRENT FEEDFORWARD

As for CCF and GCF control, system instability usually occurs around the resonant frequencies. Note that the feedforward component in the proposed scheme is the partial capacitor current with specific frequencies (e.g., 5th, 7th harmonics, etc.). Since the frequencies of the feedforward component are far below the resonant frequencies, the stable region with the proposed control scheme is almost the same as that of the conventional CCF control scheme. As a result, the proposed scheme can be concluded to have little effect on the system stability.

According to (19) , the amplitude gains of $I_C(s)$ are $20\lg(h\omega' C)$ at harmonic frequencies, while the gains decline at other frequencies, including the LCL resonant frequencies. In other words, $I_C(s)$ exhibits such attenuation characteristic which can be ideally considered to have zero gain at those frequencies except harmonic frequencies. Hence, there is no capacitor current feedforward except that at the harmonic frequencies.

To further discuss the system stability issues, the root loci method is used. Typically, a root locus diagram indicates the transfer function's pole locations for the varying values of scalar gain. Note that the root locus cannot be plotted in the s-domain since the system studied contains a delay component. Thus, the analysis is implemented in the z-domain herein. The controller transfer function can be simplified to be $G_c(s) = K_p$, since the resonant terms have negligible influence on system stability [20]. $I_C(s)$ is configured to extract the 1st, 5th and 7th order capacitor current harmonics. The system characteristic equation in z- domain can then be represented as

$$1+K_p\frac{E(z)R(z)-P(z)Q(z)}{\omega_r L_1(L_1+L_2)(z-1)z[z^2-2z\cos(\omega_r T_s)+1]R(z)}=0 \tag{23}$$

where $G_5(z) = \frac{Q(z)}{R(z)}$, $P(z) = \sin(\omega_r T_s)(L_1 + L_2)(z-1)^2$, $E(z) = \omega_r L_1 T_s[z^2 - 2z\cos(\omega_r T_s)+1]+L_2\sin(\omega_r T_s)(z-1)^2$.

The root loci is exhibited in Fig. 11 with four different resonance frequencies corresponding to the capacitor values shown in Table 1. In z-domain, the necessary and sufficient condition for the system stability is that there should be no pole-zero of open-loop transfer function outside the unit circle. It can be observed form Fig. 11 that the root loci cross the unit circle at the frequency of $f_s/6$, which is the boundary from stability to instability, and is the same as that of the conventional CCF control [6], [20]. However, there are some poles and zeros added compared with those of the conventional CCF control system in [9]. It can be confirmed that $R(z)$ contains no unstable poles outside the unit circle. Therefore, the stability is not affected by those

TABLE 1. LCL parameters and resonance frequencies.

Converter-side inductor L_1 (mH)	1.9			
Grid-side inductor L_2 (mH)	0.4			
Capacitor C_f (μF)	25	13.3	6.5	3.0
Resonance frequency f_r (kHz)	1.75	2.4	3.43	5.05
Control frequency f_s (kHz)	20			

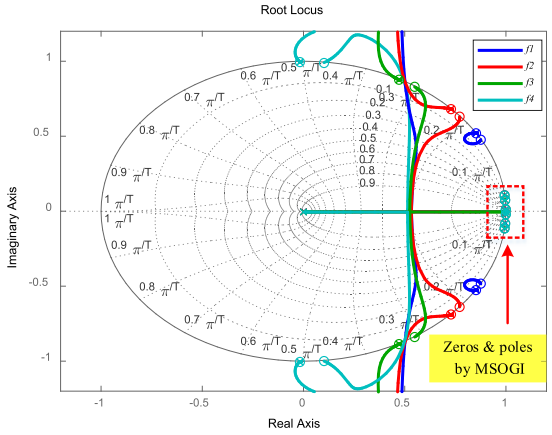

(a)

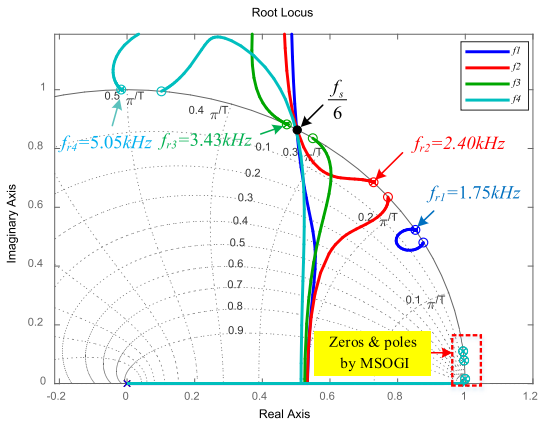

(b)

FIGURE 11. (a) Root loci of proposed scheme with four different LCL resonance frequencies, (b) the zoomed-in root loci.

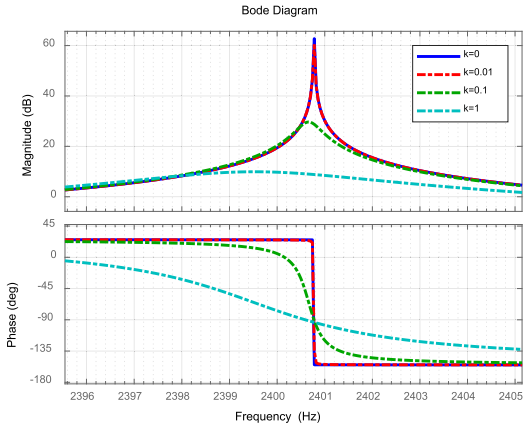

FIGURE 12. Bode diagram of proposed CCF control system with different damping gains of MSOGI.

new added poles. Consequently, the stable region is almost the same as that of the conventional CCF control system.

In order to study the slight deviation caused by the MSOGI, bode diagram is shown in Fig. 12 with different damping gains, i.e., k ($k = 0$, 0.01, 0.1 and 1) of MSOGI. Note

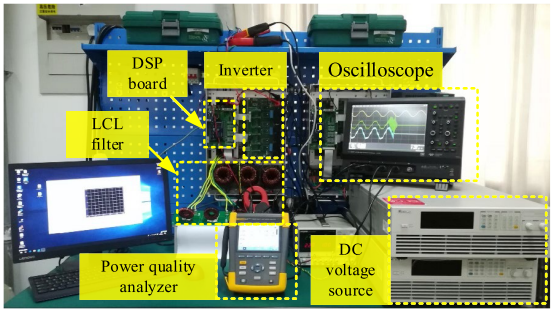

FIGURE 13. Experimental platform of Three-phase LCL-filtered grid-connected converter.

that $k = 0$ represents the conventional CCF control system. According to Fig. 12, it can be summarized that the magnitude and phase gradually approach the conventional CCF control system with k decreasing. Therefore, the slight deviation can be ignored when k is properly selected. And the stable region of the proposed scheme can thus be confirmed to $(0, f_s/6)$.

Based on the analysis, it is obvious that the proposed scheme is actually a fusion of both the CCF and GCF control, i.e., inheriting the stability characteristics of the conventional CCF control scheme and the harmonic attenuation capability of the GCF control scheme.

V. EXPERIMENTAL VALIDATIONS

In order to verify the effectiveness of the proposed control, an experimental platform of three-phase LCL grid-connected converter was constructed, as shown in Fig. 13. The platform is rated at 5kW with the first set of parameters shown in Tab.1.

The measuring equipment are the Teledyne LeCroy-HDO4024 oscilloscope and the Fluke 435 II power quality analyzer. Texas Instruments TMS320F28335 DSP is used to implement the control algorithm including MSOGI and *HCs*. The switching frequency of the converter is 20 kHz with 2us dead time.

During the test, the grid voltage is harmonically distorted with the 5^{th}, 7^{th}, 11^{th} and 13^{th} harmonics at THD 2.1%. And the MSOGI is thus configured at the fundamental and 5^{th}, 7^{th}, 11^{th}, and 13^{th} harmonics. When the converter current is zero, all the grid current flows into the filter capacitor through the grid-side inductor, at which time the capacitor voltage is sampled to extract the current. Fig. 14 shows the measured capacitor current waveform, i.e., i_c by the current sensor and the extracted current waveform, i.e., i_c' based on the MSOGI. As shown, the current error, i.e. $(i_c - i_c')$, is almost zero. The accuracy of the capacitor current extraction method based on MSOGI is thus verified.

Fig. 15 shows the experimental waveforms of the grid current and the converter current with the proposed CCF control and conventional GCF control. It can be observed that the system is stable when the partial capacitor current compensated. However, when the GCF control is applied, the converter current oscillates and triggers the overcurrent

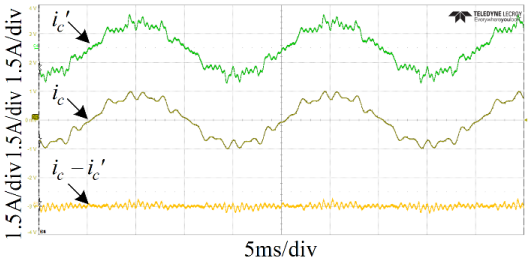

FIGURE 14. Extracted capacitor-current waveform based on MSOGI and measured capacitor-current waveform.

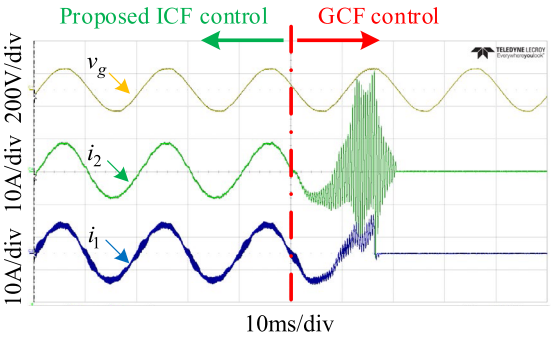

FIGURE 15. Experimental waveforms of the grid current and the converter current of proposed CCF control and GCF control.

protection eventually. The effectiveness and feasibility of the proposed control are hence demonstrated.

The closed-loop experiment test is then carried out and the current reference is set to be 10A. Fig. 16 shows the experimental waveforms of the grid voltage, converter current and grid current under different control schemes, i.e., (a) conventional CCF control without HCs, (b) conventional CCF control with HCs and (c) proposed control, respectively. To show the harmonics clearly, the spectrum analysis is applied and the FFT of grid current is also shown in Fig. 16. As shown in Fig. 16(a), when the conventional CCF control is performed, the grid current is seriously distorted by the gird background harmonics, and the THD reaches up to 8.3% with amount of 5th, 7th, 11th and 13th harmonics. When the harmonic controller HCs (configured as 5th, 7th, 11th and 13th harmonics) is applied, however, as shown Fig. 16(b),

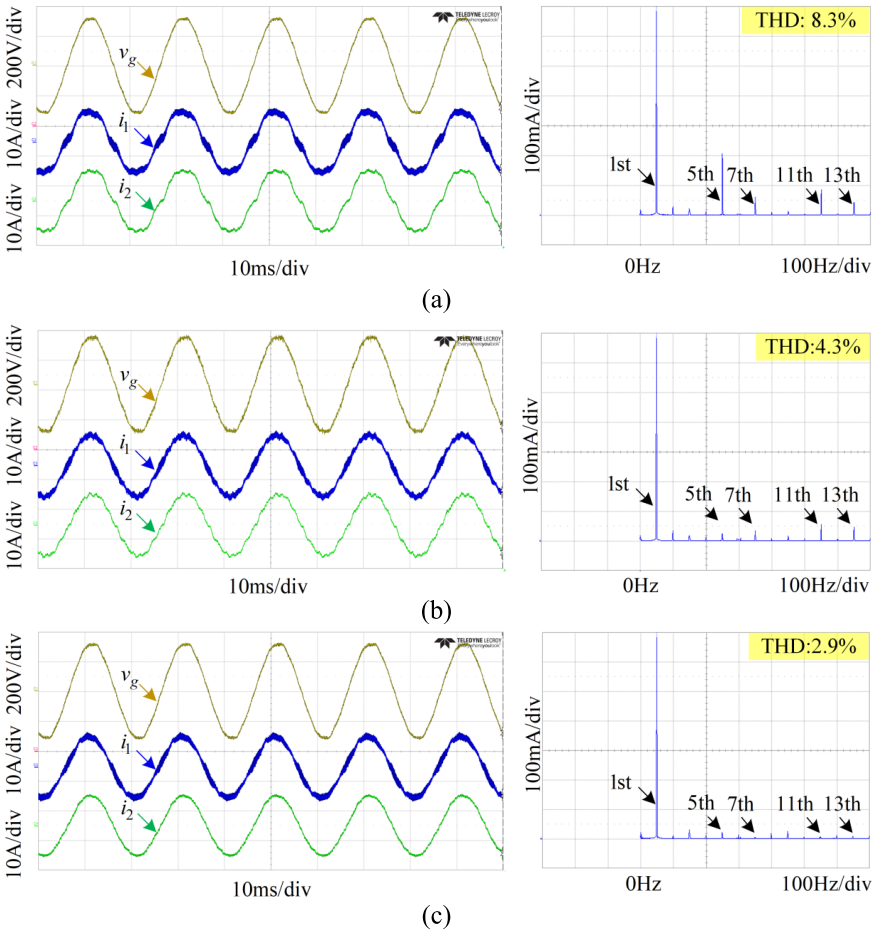

FIGURE 16. Experimental waveforms of the grid voltage, converter current and grid current and the FFT of grid current based on different control methods. (a) Conventional CCF control without HCs, (b) Conventional CCF control with HCs, (c) proposed CCF control.

the grid current is significantly improved, and the THD is reduced to be 4.3%. Note that the grid current still contains certain amount of harmonic current since no grid background harmonic information is feedback in such control system. As a contrast, when the proposed control is employed, the grid current THD reduces to be 2.9%, and the system is stable without any oscillations, as shown in Fig. 16(c). Consequently, the harmonic suppression capability and system stability of the proposed control are validated.

VI. CONCLUSIONS

This paper analyses the influence of grid background harmonics on the grid current of grid-connected PWM converters with LCL filters. To suppress the harmonic current, an improved CCF control scheme with partial capacitor current feedforward is proposed, which inherits the superior stability characteristics of CCF control scheme and the excellent capability of harmonic suppression of the GCF control scheme. The system harmonic impendence is modeling and discussed to study the harmonic suppression capability. And in term of the system stability, the root loci method is applied, and the stability is verified to be the same as that of the conventional CCF control scheme. Since the capacitor current is extracted by the MSOGI, no extra current sensors are needed. Experimental results verified the effectiveness and feasibility of the proposed control scheme.

REFERENCES

[1] M. Liserre, F. Blaabjerg, and S. Hansen, "Design and control of an LCL-filter-based three-phase active rectifier," *IEEE Trans. Ind. Appl.*, vol. 41, no. 5, pp. 1281–1291, Sep./Oct. 2005.
[2] Y. He, H. S.-H. Chung, C. N.-M. Ho, and W. Wu, "Direct current tracking using boundary control with second-order switching surface for three-phase three-wire grid-connected inverter," *IEEE Trans. Power Electron.*, vol. 32, no. 7, pp. 5723–5740, Jul. 2017.
[3] Y. Tang, W. Yao, P. C. Loh, and F. Blaabjerg, "Design of LCL filters with LCL resonance frequencies beyond the Nyquist frequency for grid-connected converters," *IEEE Trans. Emerg. Sel. Topics Power Electron.*, vol. 4, no. 1, pp. 3–14, Mar. 2016.
[4] L. Iman, A. A. Hossein, S. Mehdi, B. Alireza, and M. G. Josep, "Capacitor current feedback-based active resonance damping strategies for digitally-controlled inductive-capacitive-inductive-filtered grid-connected inverters," *Energies*, vol. 9, no. 8, p. 642, 2016.
[5] Y. Liu and C.-M. Lai, "LCL filter design with EMI noise consideration for grid-connected inverter," *Energies*, vol. 11, no. 7, p. 1646, 2018.
[6] S. G. Parker, B. P. McGrath, and D. G. Holmes, "Regions of active damping control for LCL filters," *IEEE Trans. Ind. Appl.*, vol. 50, no. 1, pp. 424–432, Jan./Feb. 2014.
[7] Q. Yan, X. Wu, X. Yuan, and Y. Geng, "An improved grid-voltage feedforward strategy for high-power three-phase grid-connected inverters based on the simplified repetitive predictor," *IEEE Trans. Power Electron.*, vol. 31, no. 5, pp. 3880–3897, May 2016.
[8] T. Abeyasekera, C. M. Johnson, D. J. Atkinson, and M. Armstrong, "Suppression of line voltage related distortion in current controlled grid connected inverters," *IEEE Trans. Power Electron.*, vol. 20, no. 6, pp. 1393–1401, Nov. 2005.
[9] Z. Xin, X. Wang, P. C. Loh, and F. Blaabjerg, "Grid-current-feedback control for LCL-filtered grid converters with enhanced stability," *IEEE Trans. Power Electron.*, vol. 32, no. 4, pp. 3216–3228, Apr. 2017.
[10] W. Jin, Y. Li, G. Sun, and L. Bu, "H∞ repetitive control based on active damping with reduced computation delay for lcl-type grid-connected inverters," *Energies*, vol. 10, no. 5, p. 586, 2017.
[11] N. Zhang, H. Tang, and C. Yao, "A systematic method for designing a PR controller and active damping of the LCL filter for single-phase grid-connected PV inverters," *Energies*, vol. 7, no. 6, pp. 3934–3954, 2014.
[12] Y. Cho, B.-J. Byen, H.-S. Lee, and K.-Y. Cho, "A single-loop repetitive voltage controller with an active damping control technique," *Energies*, vol. 10, no. 5, p. 673, 2017.
[13] J. Dannehl, M. Liserre, and F. W. Fuchs, "Filter-based active damping of voltage source converters with *LCL* filter," *IEEE Trans. Ind. Electron.*, vol. 58, no. 8, pp. 3623–3633, Aug. 2011.
[14] Y. Tang, P. C. Loh, P. Wang, F. H. Choo, F. Gao, and F. Blaabjerg, "Generalized design of high performance shunt active power filter with output LCL filter," *IEEE Trans. Ind. Electron.*, vol. 59, no. 3, pp. 1443–1452, Mar. 2012.
[15] G. Escobar, M. J. Lopez-Sanchez, D. F. Balam-Tamayo, J. A. Alonzo-Chavarria, and J. M. Sosa, "Inverter-side current control of a single-phase inverter grid connected trough an LCL filter," in *Proc. 40th Annu. Conf. IEEE Ind. Electron. Soc. (IECON)*, Dallas, TX, USA, Oct./Nov. 2014, pp. 5552–5558.
[16] W. Yao, X. Wang, P. C. Loh, X. Zhang, and F. Blaabjerg, "Improved power decoupling scheme for a single-phase grid-connected differential inverter with realistic mismatch in storage capacitances," *IEEE Trans. Power Electron.*, vol. 32, no. 1, pp. 186–199, Jan. 2017.
[17] T. Liu, X. Hao, X. Yang, M. Zhao, and L. S. Xiong, "A novel grid voltage feedforward control strategy for grid-connected inverters in weak grid," in *Proc. 43rd Annu. Conf. IEEE Ind. Electron. Soc. (IECON)*, Beijing, China, Oct./Nov. 2017, pp. 627–632.
[18] Z. Xin, P. Mattavelli, W. Yao, Y. Yang, F. Blaabjerg, and P. C. Loh, "Mitigation of grid-current distortion for LCL-filtered voltage-source inverter with inverter-current feedback control," *IEEE Trans. Power Electron.*, vol. 33, no. 7, pp. 6248–6261, Jul. 2018.
[19] J. Dannehl, F. W. Fuchs, S. Hansen, and P. B. Thøgersen, "Investigation of active damping approaches for PI-based current control of grid-connected pulse width modulation converters with LCL filters," *IEEE Trans. Ind. Appl.*, vol. 46, no. 4, pp. 1509–1517, Jul./Aug. 2010.
[20] J. Wang, J. D. Yan, L. Jiang, and J. Zou, "Delay-dependent stability of single-loop controlled grid-connected inverters with *LCL* filters," *IEEE Trans. Power Electron.*, vol. 31, no. 1, pp. 743–757, Jan. 2016.
[21] Z. Zeng *et al.*, "Analysis on controller of grid-connected inverter by using virtual circuit," in *Proc. 17th Eur. Conf. Power Electron. Appl. (ECCE-Eur.)*, Geneva, Switzerland, Sep. 2015, pp. 1–8.
[22] D. G. Holmes, T. A. Lipo, B. P. McGrath, and W. Y. Kong, "Optimized design of stationary frame three phase AC current regulators," *IEEE Trans. Power Electron.*, vol. 24, no. 11, pp. 2417–2426, Nov. 2009.
[23] P. Rodriguez, A. Luna, I. Candela, R. Teodorescu, and F. Blaabjerg, "Grid synchronization of power converters using multiple second order generalized integrators," in *Proc. 34th Annu. Conf. IEEE Ind. Electron.*, Orlando, FL, USA, Nov. 2008, pp. 755–760.

RENDE ZHAO (M'15) received the B.S. and M.S. degrees in electrical engineering from Shandong University, Jinan, China, in 1999 and 2002, respectively, and the Ph.D. degree from Zhejiang University, Hangzhou, China, in 2005.

Since 2006, he has been an Associate Professor with the China University of Petroleum, Qingdao, China. His research interests include renewable energy generation and motor control.

QIAN LI received the B.S. degree from the College of Information and Control Engineering, China University of Petroleum, Qingdao, China, in 2016, where he is currently pursuing the M.S. degree. His current research interests include power quality and modeling and control of power converters for renewable energy systems.

HAILIANG XU (S'10–M'14) received the B.S. degree in electrical engineering from the China University of Petroleum, Qingdao, China, in 2008, and the Ph.D. degree in electrical engineering from Zhejiang University, Hangzhou, China, in 2014.

Since 2018, he has been an Associate Professor with the China University of Petroleum. His current research interests include wind power generation, microgrid, and power quality.

YANSONG WANG received the B.S. degree in electrical engineering from Shandong University, Jinan, China, in 1988, and the M.S. degree and the Ph.D. degree in electrical engineering from the China University of Petroleum, Qingdao, China, in 1998 and 2005, respectively.

She is currently a Professor with the China University of Petroleum. Her current research interests include power quality analysis, harmonic suppression, power grid optimization planning, power network fault diagnosis, and power load forecasting.

JOSEP M. GUERRERO (S'01–M'04–SM'08–F'15) received the B.S. degree in telecommunications engineering, the M.S. degree in electronics engineering, and the Ph.D. degree in power electronics from the Technical University of Catalonia, Barcelona, Spain, in 1997, 2000, and 2003, respectively.

Since 2011, he has been a Full Professor with the Department of Energy Technology, Aalborg University, Aalborg, Denmark, where he is responsible for the Microgrid Research Program.

His research interests include power electronics, distributed energy storage systems, hierarchical and cooperative control, energy management systems, smart metering, and the Internet of Things for ac/dc microgrids; recently specially focused on maritime microgrids for electrical ships, vessels, ferries, and seaports.

Dr. Guerrero is an Associate Editor of the IEEE TRANSACTIONS ON POWER ELECTRONICS, the IEEE TRANSACTIONS ON INDUSTRIAL ELECTRONICS, and the *IEEE Industrial Electronics Magazine* and an Editor of the IEEE TRANSACTIONS ON SMART GRID.